Rapid Communications

# Emergent superconductivity in single-crystalline $MgTi_2O_4$ films via structural engineering

Wei Hu,[1,2,*] Zhongpei Feng,[3,1,*] Ben-Chao Gong,[4,*] Ge He,[1,2] Dong Li,[1,2] Mingyang Qin,[1,2] Yujun Shi,[1,2] Qian Li,[1] Qinghua Zhang,[1,3] Jie Yuan,[1,3,†] Beiyi Zhu,[1] Kai Liu,[4] Tao Xiang,[1,2] Lin Gu,[1,2,3] Fang Zhou,[1,2,3] Xiaoli Dong,[1,2,3] Zhongxian Zhao,[1,2,3] and Kui Jin[1,2,3,‡]

[1]*Beijing National Laboratory for Condensed Matter Physics, Institute of Physics, Chinese Academy of Sciences, Beijing 100190, China*
[2]*School of Physical Sciences, University of Chinese Academy of Sciences, Beijing 100049, China*
[3]*Songshan Lake Materials Laboratory, Dongguan, Guangdong 523808, China*
[4]*Department of Physics and Beijing Key Laboratory of Opto-electronic Functional Materials & Micro-nano Devices, Renmin University of China, Beijing 100872, China*

(Received 10 June 2019; accepted 4 June 2020; published 30 June 2020)

Spinel compounds have exhibited rich functionalities but have rarely shown superconductivity. Here, we report the emergence of superconductivity in the spinel $MgTi_2O_4$, known to be an insulator with a complicated order. The superconductivity is achieved by engineering a superlattice of $MgTi_2O_4$ and $SrTiO_3$. The onset transition temperature in the $MgTi_2O_4$ layer can be tuned from 0 to 5 K in such a geometry, concurrently with a stretched out-of-plane lattice (from 8.51 to 8.53 Å) compared to the bulk material. Such a positive correlation suggests ample room for further enhancement. Intriguingly, the superlattice exhibits an isotropic upper critical field $B_{c2}$ that breaks the Pauli limit, distinct from the highly anisotropic feature of interface superconductivity. The origin of superconductivity in the $MgTi_2O_4$ layer is understood in combination with the electron energy loss spectra and first-principles electronic structure calculations, which point to the birth of superconductivity by suppressing orbital ordering. Our discovery not only provides a platform to explore the interplay between superconductivity and other exotic states, but also opens another window to realize superconductivity in spinel compounds as well as other titanium oxides.

DOI: 10.1103/PhysRevB.101.220510

Exploring new superconductors in a family of materials with rich functionalities not only assists in unraveling the interplay between superconductivity and other exotic states, but also enriches diverse applications. The spinel family has shown rich functionalities, such as a multiferroic effect [1], anomalous magnetotransport [2], large magnetostriction [3], oxygen evolution catalysis [4], and high-profile electrode performance [5]. In addition, novel phenomena have been disclosed in some materials, e.g., a heavy electron feature in $LiV_2O_4$ [6,7], charge ordering in $AlV_2O_4$ [8], spin fluctuations in $ZnCr_2O_4$ [9], an orbital glass state in $Co_{1+x}V_{2-x}O_4$ [10], and orbital ordering in $CuIr_2S_4$ [11] and $MgTi_2O_4$ (MTO) [12–15]. Nevertheless, so far only $LiTi_2O_4$ (LTO) has been reported to be a superconductor among the spinel oxides, which was discovered half a century ago [16]. Subsequent research on LTO gradually unveiled the novel superconductivity in spinel oxides, such as an orbital-related state above the superconducting transition and the anomalies of the upper critical field [17–20]. However, a further comprehensive study requires its counterparts. Discovering more spinel oxide superconductors has always been challenging, but may open another source comparable to the families of copper-oxide and Fe-based superconductors [21,22].

Since there are many similarities between MTO and LTO, e.g., an approximate ionic radius between $Mg^{2+}$ and $Li^{+}$, one would expect that MTO might also show superconductivity. Considerable efforts have been made in the past several decades, for instance, adjusting the Mg/Ti ratio or substituting Mg by La [23–26]. However, it has not been successful in turning MTO into a superconductor. Indeed, the bulk MTO undergoes a simultaneous metal-to-insulator and cubic-to-tetragonal transition on cooling at 260 K [12–15]. Meanwhile, the formation of orbital ordering, resulting from the helical dimerization pattern of alternating short and long Ti-Ti bonds, is responsible for the band-insulator nature of the low-temperature tetragonal phase [14]. Theoretical studies have also mentioned the existence of a valence-bond crystal [27] and orbitally induced Peierls state [15] in MTO. Thus, it seems unrealistic for the appearance of superconductivity in such a "robust" insulator. Nevertheless, it should be noted that the suppression of ordered states, e.g., antiferromagnetic order in cuprates [21], nematic order in Fe-based superconductors [28], and charge-density waves in $Cu_xTiSe_2$ [29], is a feasible approach to explore different superconductors. While good control of the chemical composition of single-crystal MTO is challenged by the thermodynamic instability of the crystal lattice, single-crystalline MTO could be stabilized in the form of thin films on a lattice-matched single-crystal substrate, similar to LTO [18]. Owing to the strong-coupling feature of transition metal oxide, the orbital ordering can be effectively modulated via stoichiometry control or epitaxial strain [30]. Therefore, the emergence of superconductivity in MTO films is promising.

As shown in this Rapid Communication, the resistance can be greatly reduced in our single-crystalline MTO films

*These authors contributed equally to this work.
†yuanjie@iphy.ac.cn
‡kuijin@iphy.ac.cn

 

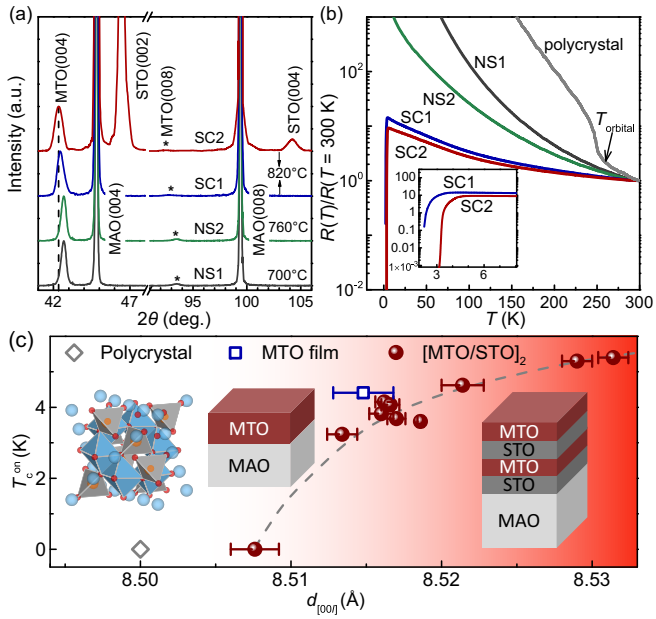


FIG. 1. (a) XRD spectra of $\theta$-$2\theta$ scanning. The curves are shifted vertically for clarity. Samples named NS1, NS2, and SC1 are selected MTO film samples directly grown on a MAO substrate with different deposition temperatures from 700 to 820°C. The sample SC2 is a $[MTO/STO]_2$ superlattice with two ~40-nm periods of STO and MTO layers on MAO. (b) Temperature dependence of normalized resistance for NS1, NS2, SC1, SC2, and the MTO polycrystal [26]. $T_{orbital}$ represents the temperature at which the orbital ordering steps into the MTO bulk. Inset: Zoom-in low-temperature resistance of SC1 and SC2 samples. (c) The onset superconducting transition temperature vs out-of-plane lattice constant $d_{[00l]}$ of MTO. The data points, i.e., open diamond, open squares, and solid circles, are extracted from the polycrystal, the MTO films, and the superlattices, respectively. Insets from left to right: MTO unit cell, schematic structures of the thin film, and the superlattice. The film thickness is ~80 nm in the single-layer configuration.

by adjusting the growth parameters. Remarkably, there is an indication of superconductivity starting at ~3.5 K in the less resistive sample. To achieve a full superconducting transition, we further engineer the MTO via a superlattice architecture, composed of MTO and $SrTiO_3$ (STO) layers [inset of Fig. 1(c)]. The transition to zero resistance is successfully realized, with the best onset temperature ($T_c^{on}$) up to 5 K.

Our MTO thin films and MTO/STO superlattices were grown on (00$l$)-oriented cubic spinel $MgAl_2O_4$ (MAO) substrates by the pulsed laser deposition (PLD) method. MAO has a smaller lattice constant of 8.08 Å than bulk MTO (~8.50 Å), which can provide a compressive in-plane strain on the MTO film. The STO and MTO layers were deposited by ablating a home-made $SrTiO_3$ target and a commercial $MgTi_2O_5$ target (for that the $MgTi_2O_4$ target is unstable). All the samples were grown in a high vacuum of better than $1 \times 10^{-6}$ Torr, with a pulse energy of ~250 mJ and a repetition rate of 4 Hz. The deposition temperature was set in the range from 680 to 820°C. The crystal structures for all the samples were examined on a commercial x-ray diffractometer. X-ray diffraction (XRD) results reveal that the MTO is well oriented along the [00$l$] direction either on the MAO substrate or adjacent to the STO layer in the superlattice. The epitaxial growth of MTO films was also confirmed by x-ray $\varphi$-scan and reciprocal space mapping (see Supplemental Material [31], Fig. S2). The thickness of each layer was examined by scanning transmission electron microscopy (STEM) from the cross-section images. Transport and magnetization measurements were performed in a physical property measurement system (magnetic field up to 9 T) and magnetic property measurement system (remnant field less than 4 mOe), respectively. The standard van der Pauw method was employed for the resistance measurement.

For the MTO film on MAO, the out-of-plane lattice constant $d_{[00l]}$ could be tuned from ~8.44 to ~8.52 Å, as manifested by the obvious shift of the (004) Bragg peak to a lower angle from the NS1 to SC1 samples in Fig. 1(a). Such an evolution is mainly caused by varying the deposition temperature. Following a stretched $d_{[00l]}$, the MTO films become more conductive. Finally, an abrupt drop of the resistance is observed around 3.5 K (sample SC1) with decreasing temperature as shown in Fig. 1(b). This is an indication of a superconducting transition, albeit not complete. In such a case, the superconducting regions in the film are not connected and a clean Meissner effect cannot be observed in the magnetization measurement. Nevertheless, it suggests that further increasing the $d_{[00l]}$ may enhance the $T_c^{on}$ and realize a complete superconducting transition. Such an idea is accomplished by *in situ* growing STO and MTO layers alternately to form a $[MTO/STO]_2$ superlattice, in which the $d_{[00l]}$ of MTO in superlattices could be tuned in a wider range up to 8.53 Å. For the sample with the largest $d_{[00l]}$ value [SC2 in Fig. 1(b)], zero resistance can be achieved at 3 K and the onset transition temperature reaches up to 5 K. Our x-ray data show a remarkable link between the out-of-plane $d$ spacing and the emergence of superconductivity in our films and superlattices [Fig. 1(c)]. Systematic structure and transport characterizations of samples deposited at various temperatures are provided in the Supplemental Material [31] (Fig. S1). It is worth pointing out that the MTO layers grown at higher temperatures always have enhanced $d_{[00l]}$ and $T_c^{on}$ values, both in single-layer films and in $[MTO/STO]_2$ superlattices. Such a positive correlation between the out-of-plane lattice parameter and the $T_c^{on}$ has also been found in the high-$T_c$ superconductors, such as in (Li,Fe)OHFeSe [32] and in $La_{2-x}Sr_xCuO_4$ heterostructures [33]. We also notice that the orbital ordering in bulk MTO is significantly suppressed in our single-crystalline films and superlattices, evident from the smeared kink in the resistance curve [Fig. 1(b)].

To confirm that the zero resistance indeed comes from a superconducting transition, we also carried out magnetotransport and magnetization measurements. Figure 2(a) clearly shows that the magnetic field, applied perpendicular to the film ($B \perp$ film, i.e., parallel to the [00$l$] direction) from 0 to 9 T, gradually restrains the superconductivity. Meanwhile, the temperature dependence of the magnetic susceptibility in both zero-field-cooling and field-cooling modes discloses that the Meissner state appears at 3 K [Fig. 2(b)], consistent with the zero-resistance transition temperature. The superconductivity in superlattice or multilayer structures usually shows an anisotropic $B_{c2}$, which is used to support a lower-dimensional superconductivity confined at the interfaces, e.g.,

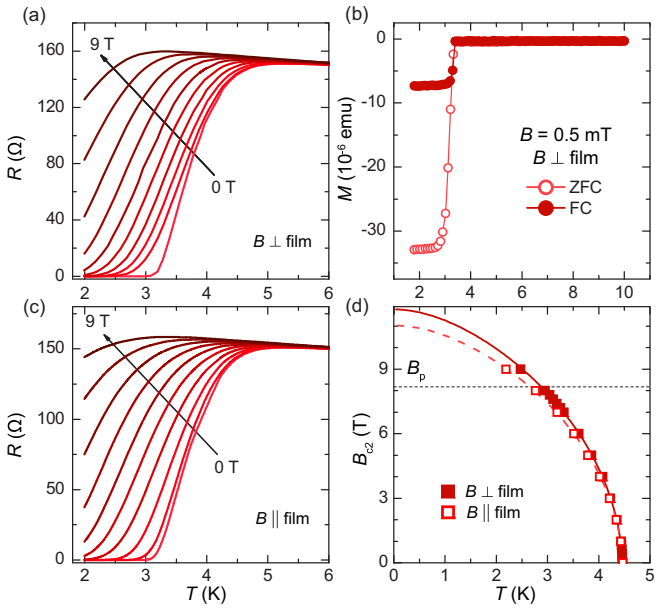


FIG. 2. (a) Temperature dependence of electrical resistance of the $[MTO/STO]_2$ superlattice under various magnetic fields perpendicular to the film. (b) Temperature dependence of magnetization of the $[MTO/STO]_2$ superlattice at 0.5 mT with and without field cooling. (c) Temperature dependence of electrical resistance of the $[MTO/STO]_2$ superlattice under various magnetic fields parallel to the film. (d) Temperature-dependent upper critical field $B_{c2}$ of the $[MTO/STO]_2$ superlattice with $B \perp$ film (solid squares) and $B \parallel$ film (open squares). Solid and dashed lines are fits by the WHH theory. The Pauli limit $B_p$ is marked by the dashed horizontal line.

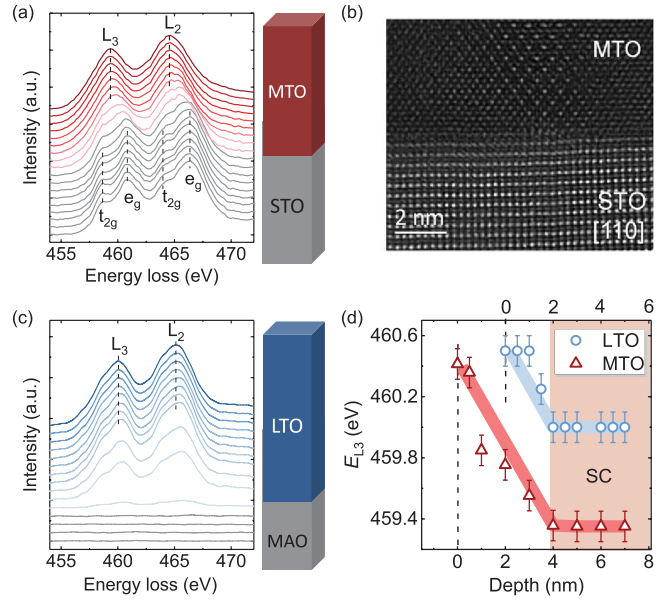


FIG. 3. (a) EELS profiles for Ti $L_{2,3}$ edges of the $[MTO/STO]_2$ superlattice. The curves are shifted vertically from the STO layer to MTO layer. (b) High-angle annular dark-field (HAADF) STEM image of the superlattice. (c) EELS profiles for Ti $L_{2,3}$ edges of the LTO film on the MAO substrate. (d) The depth dependence of the peak position of the Ti $L_3$ edge (noted as $E_{L3}$). The data are extracted from the EELS profiles and the depth of the interface is offset to 0.

in $LaAlO_3/SrTiO_3$ [34–37], in surface superconducting $MoS_2$ by ionic liquid gating [38]. Therefore, the resistance in magnetic fields parallel to the film ($B \parallel$ film, i.e., perpendicular to the $[00l]$ direction) is also measured as shown in Fig. 2(c). Surprisingly, the magnetoresistance shows similar behavior to the case of $B \perp$ film, pointing to a roughly isotropic $B_{c2}$. As seen in Fig. 2(d), the temperature dependence of $B_{c2}$ can be well fitted by the Werthamer-Helfand-Hohenberg (WHH) theory if spin paramagnetism and the spin-orbit interaction are taken into consideration, where the Ginzburg-Landau coherence length $\xi_{GL}$ of the MTO layer can be estimated to be ~1.78 nm [39]. Here, the value of $B_{c2}$ is defined as the field where the resistance is 90% of the normal state resistance. The $B_{c2}$ ($T = 0$) is between 11 and 12 T, well above the Pauli limit ($B_p = 1.84T_c$, given by the weak-coupling BCS paramagnetic formula, where $T_c$ is defined as the temperature where the resistance drops to 90% of the normal state resistance). Breaking the Pauli limit has been constantly observed in (quasi-)two-dimensional systems, which can provide valuable information to understand the pairing breaking and ordering symmetry, but the $B_{c2}$ is highly anisotropic [35,38]. An isotropic $B_{c2}$ in a centrosymmetric system that breaks the Pauli limit has been rarely seen before [40], suggesting that such emergent superconductivity in the MTO layer is not intuitively confined to the interface, otherwise an anisotropic $B_{c2}$ should be expected.

The following questions naturally arise: Where does the superconducting signal come from? What is the role of the STO layer? First, STO has been reported to show superconductivity at ~200 mK when annealed in high temperature and high vacuum [41]. Such a process can remove a tiny amount of oxygen and turn partial $Ti^{4+}$ ions into $Ti^{3+}$. Spatially resolved electron energy loss spectroscopy (EELS), with a ~0.02 nm spatial increment of the line scan of the spectrum images, has been used to verify the Ti valency in our superlattice geometry. From the inner side of the STO layer to the interface, both the Ti $L_{2,3}$ edges, from $2p_{1/2}$ and $2p_{2/3}$ to $3d$ orbits, respectively, split into two peaks, corresponding to the hopping to $e_g$ and $t_{2g}$ orbits, and their energy positions do not vary as shown in Fig. 3(a). Meanwhile, a high-angle annular dark-field (HAADF) STEM image across the interface illustrates the nearly perfect STO layer [Fig. 3(b)]. This reflects that the valence of Ti is always +4, both inside the STO layer and near the interface [19]. Besides, the reported $T_c^{on}$ of STO has not yet exceeded 400 mK [42]. Hence, the observed superconducting signal at 5 K should not be from the STO layer. The isotropic upper critical field helps to rule that the superconductivity only resides at the interface. Consequently, the origin of the superconductivity should be locked to the MTO layer.

It is known that depositing LTO films in high vacuum can reduce the Li/Ti ratio [19]. Previous work on powders has found that the reduced Mg/Ti ratio in MTO can result in an expansion of the crystal lattice [24]. The results of energy-dispersive x-ray (EDX) spectrometer mapping on MTO films also suggest the decreasing tendency of the Mg/Ti ratio, as well as the enlargement of the $d_{[00l]}$ value, with an increase of deposition temperature (see Supplemental Material [31], Fig. S3). Considering that the superconductivity emerges under a

higher growth temperature, it is reasonable to speculate that the superconductivity stems from the reduced Mg/Ti ratio in our samples. However, an excessive reduction of the Mg/Ti ratio will destabilize the MTO lattice in the bulk. In the film, the MAO substrate helps to stabilize the crystal lattice as that in LTO experiments, in which the film is more stable than the bulk [18,19]. In the $[MTO/STO]_2$ superlattice, the STO layer seems to play a role in stabilizing the MTO lattice with a further reduced Mg/Ti ratio. Comparing the EELS spectra of MTO to that of STO layers, we find that it mimics the comparison between the superconducting $LiTi_2O_4$ and the insulating $Li_4Ti_5O_{12}$ [19]. With varying distances from interface, the peak position of the Ti $L_3$ edge (noted as $E_{L3}$), first shifts towards a lower energy and then saturates at 459.3 eV [Fig. 3(d)]. Intriguingly, as shown in Fig. 3(c), a similar evolution is also detected in the LTO film on the MAO substrate where the redshift of the Ti $L_3$ edge is associated with the out-of-plane lattice expansion, caused by the variation of oxygen concentration. In some sense the superlattice structure assists in engineering the electronic structure of the MTO analog to the superconducting LTO. Therefore, it is intuitive to link the decrease of $E_{L3}$ in MTO with the stretch of the out-of-plane lattice. Combined with the relation between $d_{[00l]}$ and $T_c^{on}$, we speculate that the superconducting area locates in the broad region marked by the shadow rather than the limited region adjacent to the interface [Fig. 3(d)], resulting in the isotropic $B_{c2}$. However, we should point out that with varying the out-of-plane lattice constant, the $T_c^{on}$ of MTO is tunable compared to a robust $T_c^{on}$ in LTO, which provides plenty of room for further enhancing the superconductivity in other superlattice architectures and exploring the interplay between the superconductivity and other degrees of freedom such as the orbital ordering and spin-orbit coupling.

To further understand the change of electronic properties with the structural engineering in MTO (Fig. 1), we performed spin-polarized electronic structure calculations for different MTO lattices, including the bulk and film (see the Supplemental Material for computational details [31]). Figure 4(a) shows the calculated density of states (DOS) for the tetragonal phase of bulk MTO, which exhibits semiconducting behavior, being consistent with experimental measurements [43]. It should be noted that one would obtain a metallic state unless the Hubbard interaction was included in the calculation. This indicates that the low-temperature phase of bulk MTO is a Mott insulator, in accordance with previous theoretical studies [44]. On the other hand, for the MTO film with expanded lattice constants but no doping [Fig. 4(c)], the DOS demonstrates little variation compared with the bulk case. The occupied states near the Fermi level for both cases consist of Ti $d_{xz}$ and $d_{yz}$ orbitals [Figs. 4(a) and 4(c)], which are alternatively distributed in real space in a dimerized form [Figs. 4(b) and 4(d)], i.e., possessing orbital ordering. With the electron doping by the reduced Mg/Ti ratio in the MTO film (see Supplemental Material [31], Fig. S3), the occupied states near the Fermi level involve Ti $d_{xy}$ orbitals [Figs. 4(e) and 4(f)], which tend to suppress $d_{xz}$-$d_{yz}$ orbital ordering and induce superconductivity, as evidenced by the resistance measurement [Fig. 1(b)]. The above calculation results suggest that it is the electron doping via a reduced Mg/Ti ratio, showing up as the elongated lattice constants in the experiment, that is

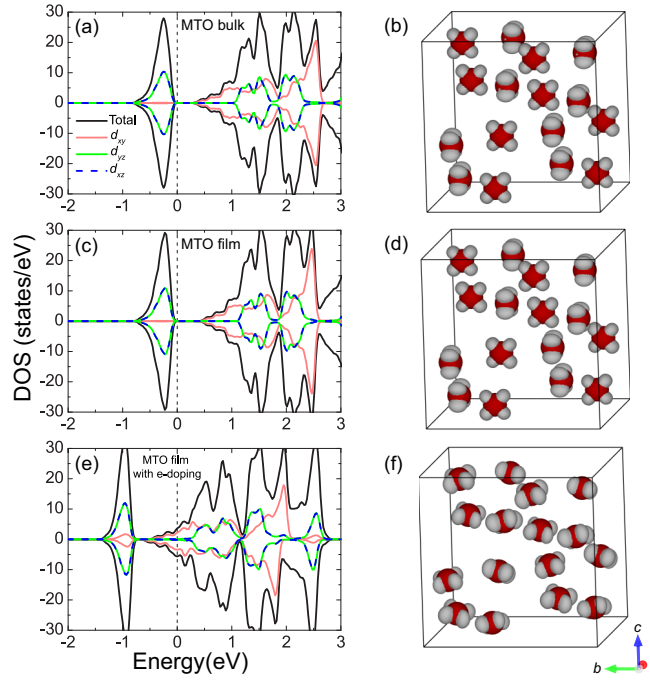


FIG. 4. Density of states (DOS) and band-decomposed charge densities in the energy range from −0.7 to 0 eV for the antiferromagnetic state of different MTO lattice parameters with a Hubbard $U$ of 2.5 eV: (a) and (b) undoped bulk MTO tetragonal phase; (c) and (d) undoped MTO film lattice; and (e) and (f) MTO film lattice with a doping concentration of 0.15 electrons per Ti atom. The Fermi level is set to zero. The detailed lattice parameters in the calculations can be seen in the Supplemental Material [31].

responsible for the suppression of orbital ordering, the closing of the band gap, and the appearance of superconductivity in the MTO film.

Overall, stable single-crystalline $MgTi_2O_4$ films have been successfully grown on the $MgAl_2O_4$ substrate, with the most conductive sample showing an indication of a superconducting transition at ∼3.5 K. As engineered in a geometry of a $[MTO/STO]_2$ superlattice, the superconducting transition with a $T_c^{on}$ of 5 K is realized in MTO. This emergent superconductivity can be linked to the reduction of the Mg/Ti ratio, accompanied by the elongation of the out-of-plane lattice, which is also consistent with the results of the first-principles electronic structure calculations. Except for providing another opportunity to discover more spinel oxide superconductors, such a discovery also generates several attractive issues: First, the superlattice shows an intriguing isotropic upper critical field up to 11 T that breaks the Pauli limit, distinct from the highly anisotropic feature of interface superconductivity as reported in the $La_{2-x}Sr_xCuO_4$ heterostructure [45], the $LaAlO_3/SrTiO_3$ [34–37], and ultrathin FeSe film on STO [46]. So it is worth considering the role of the STO layer in promoting the superconductivity from a different perspective. Second, there is a positive correlation between the $T_c^{on}$ and the out-of-plane lattice constant, so where is the upper limit and can it break the $T_c^{on}$ record of LTO in the spinel oxides? Third, besides the emergent superconductivity in MTO in the spinel structure, there are also reports of enhanced superconductivity in the perovskite $SrTiO_3$ with $TiO_6$ octahedra [42] and in

cubic titanium monoxide with wrinkled TiO planes [47], so can we find a common thread to achieve high-$T_c$ superconductivity in the titanium oxide family? We anticipate that the emergence of superconductivity in the spinel family will open a rich vein comparable to the families of copper-oxide and Fe-based superconductors.

We would like to thank L. H. Yang, Q. H. Chen, J. P. Hu, and X. H. Chen for helpful discussions. This work was supported by the National Key Basic Research Program of China (2015CB921000, 2017YFA0303003, 2017YFA0302902, 2017YFA0302903, and 2018YFB0704102), the National Natural Science Foundation of China (11674374, 11774424, 11804378, and 11834016), the Strategic Priority Research Program of Chinese Academy of Sciences (XDB25000000), the Key Research Program of Frontier Sciences, CAS (QYZDB-SSW-SLH008, QYZDY-SSW-SLH001, and QYZDB-SSW-JSC035), CAS Interdisciplinary Innovation Team, and Beijing Natural Science Foundation (Z190008). Computational resources were provided by the Physical Laboratory of High Performance Computing at Renmin University of China.

[1] J. Hemberger, P. Lunkenheimer, R. Fichtl, H.-A. K. Von Nidda, V. Tsurkan, and A. Loidl, Nature (London) **434**, 364 (2005).
[2] X. Chen, X. Zhang, M.-G. Han, L. Zhang, Y. Zhu, X. Xu, and X. Hong, Adv. Mater. **31**, 1805260 (2019).
[3] J. Hemberger, H.-A. Krug von Nidda, V. Tsurkan, and A. Loidl, Phys. Rev. Lett. **98**, 147203 (2007).
[4] Y. Liu, Y. Ying, L. Fei, Y. Liu, Q. Hu, G. Zhang, S. Y. Pang, W. Lu, C. L. Mak, X. Luo, L. Zhou, M. Wei, and H. Huang, J. Am. Chem. Soc. **141**, 8136 (2019).
[5] C. O'Rourke and B. J. Morgan, Phys. Rev. Mater. **2**, 045403 (2018).
[6] S. Kondo, D. C. Johnston, C. A. Swenson, F. Borsa, A. V. Mahajan, L. L. Miller, T. Gu, A. I. Goldman, M. B. Maple, D. A. Gajewski, E. J. Freeman, N. R. Dilley, R. P. Dickey, J. Merrin, K. Kojima, G. M. Luke, Y. J. Uemura, O. Chmaissem, and J. D. Jorgensen, Phys. Rev. Lett. **78**, 3729 (1997).
[7] C. Urano, M. Nohara, S. Kondo, F. Sakai, H. Takagi, T. Shiraki, and T. Okubo, Phys. Rev. Lett. **85**, 1052 (2000).
[8] K.-i. Matsuno, T. Katsufuji, S. Mori, Y. Moritomo, A. Machida, E. Nishibori, M. Takata, M. Sakata, N. Yamamoto, and H. Takagi, J. Phys. Soc. Jpn. **70**, 1456 (2001).
[9] S.-H. Lee, C. Broholm, W. Ratcliff, G. Gasparovic, Q. Huang, T. Kim, and S.-W. Cheong, Nature (London) **418**, 856 (2002).
[10] R. Koborinai, S. E. Dissanayake, M. Reehuis, M. Matsuda, T. Kajita, H. Kuwahara, S.-H. Lee, and T. Katsufuji, Phys. Rev. Lett. **116**, 037201 (2016).
[11] P. G. Radaelli, Y. Horibe, M. J. Gutmann, H. Ishibashi, C. Chen, R. M. Ibberson, Y. Koyama, Y.-S. Hor, V. Kiryukhin, and S.-W. Cheong, Nature (London) **416**, 155 (2002).
[12] P. G. Radaelli, New J. Phys. **7**, 53 (2005).
[13] M. Isobe and Y. Ueda, J. Phys. Soc. Jpn. **71**, 1848 (2002).
[14] M. Schmidt, W. Ratcliff, P. G. Radaelli, K. Refson, N. M. Harrison, and S. W. Cheong, Phys. Rev. Lett. **92**, 056402 (2004).
[15] D. I. Khomskii and T. Mizokawa, Phys. Rev. Lett. **94**, 156402 (2005).
[16] D. Johnston, H. Prakash, W. Zachariasen, and R. Viswanathan, Mater. Res. Bull. **8**, 777 (1973).
[17] E. G. Moshopoulou, J. Am. Ceram. Soc. **82**, 3317 (1999).
[18] K. Jin, G. He, X. Zhang, S. Maruyama, S. Yasui, R. Suchoski, J. Shin, Y. Jiang, H. Yu, J. Yuan, L. Shan, F. V. Kusmartsev, R. L. Greene, and I. Takeuchi, Nat. Commun. **6**, 7183 (2015).
[19] Y. Jia, G. He, W. Hu, H. Yang, Z. Yang, H. Yu, Q. Zhang, J. Shi, Z. Lin, J. Yuan, B. Zhu, L. Gu, H. Li, and K. Jin, Sci. Rep. **8**, 3995 (2018).
[20] Z. Wei, G. He, W. Hu, Z. Feng, X. Wei, C. Y. Ho, Q. Li, J. Yuan, C. Xi, Z. Wang, Q. Chen, B. Zhu, F. Zhou, X. Dong, L. Pi, A. Kusmartseva, F. V. Kusmartsev, Z. Zhao, and K. Jin, Phys. Rev. B **100**, 184509 (2019).
[21] N. P. Armitage, P. Fournier, and R. L. Greene, Rev. Mod. Phys. **82**, 2421 (2010).
[22] Y. Kamihara, T. Watanabe, M. Hirano, and H. Hosono, J. Am. Chem. Soc. **130**, 3296 (2008).
[23] H. Hohl, C. Kloc, and E. Bucher, J. Solid State Chem. **125**, 216 (1996).
[24] M. Isobe and Y. Ueda, J. Alloys Compd. **383**, 85 (2004).
[25] H. D. Zhou and J. B. Goodenough, Phys. Rev. B **72**, 045118 (2005).
[26] Y. Zhu, R. Wang, L. Wang, Y. Liu, R. Xiong, J. Shi, and M. Tian, J. Alloys Compd. **666**, 248 (2016).
[27] S. Di Matteo, G. Jackeli, C. Lacroix, and N. B. Perkins, Phys. Rev. Lett. **93**, 077208 (2004).
[28] R. Fernandes, A. Chubukov, and J. Schmalian, Nat. Phys. **10**, 97 (2014).
[29] E. Morosan, H. W. Zandbergen, B. Dennis, J. Bos, Y. Onose, T. Klimczuk, A. Ramirez, N. P. Ong, and R. J. Cava, Nat. Phys. **2**, 544 (2006).
[30] Y. Tokura and N. Nagaosa, Science **288**, 462 (2000).
[31] See Supplemental Material at http://link.aps.org/supplemental/10.1103/PhysRevB.101.220510 for details about structure and transport characterizations, EDX mapping analysis, and electronic structure calculations, which includes Refs. [13,14,43,48–51].
[32] X. Dong, H. Zhou, H. Yang, J. Yuan, K. Jin, F. Zhou, D. Yuan, L. Wei, J. Li, X. Wang, G. Zhang, and Z. Zhao, J. Am. Chem. Soc. **137**, 66 (2015).
[33] V. Y. Butko, G. Logvenov, N. Božović, Z. Radović, and I. Božović, Adv. Mater. **21**, 3644 (2009).
[34] N. Reyren, S. Thiel, A. D. Caviglia, L. F. Kourkoutis, G. Hammerl, C. Richter, C. W. Schneider, T. Kopp, A.-S. Rüetschi, D. Jaccard, M. Gabay, D. A. Muller, J.-M. Triscone, and J. Mannhart, Science **317**, 1196 (2007).
[35] M. Ben Shalom, M. Sachs, D. Rakhmilevitch, A. Palevski, and Y. Dagan, Phys. Rev. Lett. **104**, 126802 (2010).
[36] J. Mannhart and D. G. Schlom, Science **327**, 1607 (2010).
[37] D. Stornaiuolo, C. Cantoni, G. M. De Luca, R. Di Capua, E. Di Gennaro, G. Ghiringhelli, B. Jouault, D. Marrè, D. Massarotti,

F. M. Granozio, I. Pallecchi, C. Piamonteze, S. Rusponi, T. Tafuri, and M. Salluzzo, Nat. Mater. **15**, 278 (2016).

[38] J. M. Lu, O. Zheliuk, I. Leermakers, N. F. Q. Yuan, U. Zeitler, K. T. Law, and J. T. Ye, Science **350**, 1353 (2015).

[39] N. R. Werthamer, E. Helfand, and P. C. Hohenberg, Phys. Rev. **147**, 295 (1966), where the Ginzburg-Landau coherence length $\xi_{GL}$ can be estimated by using the zero-temperature relation $B_{c2}^{orb} = \phi_0/(2\pi\xi_{GL}^2)$. Here, $B_{c2}^{orb} = -0.69T_c(dB_{c2}/dT)|_{T_c}$ denotes the upper critical field considering orbital effects only.

[40] Ø. Fischer, Appl. Phys. **16**, 1 (1978).

[41] J. F. Schooley, W. R. Hosler, and M. L. Cohen, Phys. Rev. Lett. **12**, 474 (1964).

[42] K. Ueno, S. Nakamura, H. Shimotani, A. Ohtomo, N. Kimura, T. Nojima, H. Aoki, Y. Iwasa, and M. Kawasaki, Nat. Mater. **7**, 855 (2008).

[43] J. Zhou, G. Li, J. L. Luo, Y. C. Ma, D. Wu, B. P. Zhu, Z. Tang, J. Shi, and N. L. Wang, Phys. Rev. B **74**, 245102 (2006).

[44] S. Leoni, A. N. Yaresko, N. Perkins, H. Rosner, and L. Craco, Phys. Rev. B **78**, 125105 (2008).

[45] A. Gozar, G. Logvenov, L. F. Kourkoutis, A. Bollinger, L. Giannuzzi, D. Muller, and I. Bozovic, Nature (London) **455**, 782 (2008).

[46] Q.-Y. Wang, Z. Li, W.-H. Zhang, Z.-C. Zhang, J.-S. Zhang, W. Li, H. Ding, Y.-B. Ou, P. Deng, K. Chang, J. Wen, C.-L. Song, K. He, J.-F. Jia, S.-H. Ji, Y.-Y. Wang, L.-L. Wang, X. Chen, X.-C. Ma, and Q.-K. Xue, Chin. Phys. Lett. **29**, 037402 (2012).

[47] C. Zhang, F. Hao, G. Gao, X. Liu, C. Ma, Y. Lin, Y. Yin, and X. Li, npj Quantum Mater. **2**, 2 (2017).

[48] P. E. Blöchl, Phys. Rev. B **50**, 17953 (1994); G. Kresse and D. Joubert, *ibid.* **59**, 1758 (1999).

[49] G. Kresse and J. Hafner, Phys. Rev. B **47**, 558 (1993); J. Phys.: Condens. Matter **6**, 8245 (1994); G. Kresse and J. Furthmüller, Phys. Rev. B **54**, 11169 (1996); Comput. Mater. Sci. **6**, 15 (1996).

[50] J. P. Perdew, K. Burke, and M. Ernzerhof, Phys. Rev. Lett. **77**, 3865 (1996).

[51] S. L. Dudarev, G. A. Botton, S. Y. Savrasov, C. J. Humphreys, and A. P. Sutton, Phys. Rev. B **57**, 1505 (1998).